

pubs.acs.org/JPCB Article

# Strong Enantiomeric Preference on the Macroion—Counterion Interaction Induced by Weakly Associated Chiral Counterions

Ehsan Raee, Hui Li, Xinyu Sun, Putu Ustriyana, Jiancheng Luo, Jiahui Chen, Nita Sahai, and Tianbo Liu\*



Cite This: J. Phys. Chem. B 2020, 124, 9958–9966



**ACCESS** 

Metrics & More

Article Recommendations

Supporting Information

ABSTRACT: The role of chiral counterions on the attraction and self-assembly of chiral Pd<sub>12</sub>L<sub>24</sub> metal organic cages (MOCs) with NO<sub>3</sub><sup>-</sup> being the original counterion is studied by laser light scattering and isothermal titration calorimetry. Nitrates can trigger the self-assembly of macrocationic Pd<sub>12</sub>L<sub>24</sub> into hollow spherical blackberry-type supramolecular structures *via* counterion-mediated attraction. Although chiral counteranions, such as *N*-(*tert*-butoxycarbonyl)-alanine (Boc-Ala), have weaker interaction with the MOCs compared to NO<sub>3</sub><sup>-</sup>, they can induce different assembly behaviors between two enantiomeric MOCs by inhibiting the MOC–nitrate binding and weakening the interaction between them. The D-counterions are capable of selectively suppressing and



slowing down the assembly of L-MOCs and also considerably decreasing their assembly size due to the much weaker MOC—nitrate interaction. The same scenario is observed for L-counterions when interacting with the D-MOCs. This study unveils the role of weakly associated chiral counterions on the central chiral macroions, especially their supramolecular structure formation, and provides additional evidence on the mechanism of the homochirality phenomenon.

#### ■ INTRODUCTION

Chirality is an intriguing topic with many remaining puzzles, such as the interaction between chiral molecules, especially during their self-assembly into supramolecular structures. Pasteur first observed chirality in crystallized sodium ammonium tartrate. The enantiomers of a chiral molecule might behave differently in the biological system which is the reason for many inspiring phenomena in nature, including homochirality, that is, living organisms utilize one enantiomer of chiral biomolecules, for example, L-amino acids in proteins and D-sugars in nucleic acids. Several possibilities were presented for the origin of homochirality. 2-6 Although we are not sure about the exact origin of the phenomena, we know that formation of homochiral structures certainly involves recognition and selection of enantiomers and other chiral molecules during their organization into supramolecular structures.<sup>7-9</sup> Different mechanisms are proposed to explain chiral recognition and selection such as the "three-point" interaction model by Easson and Stedman. 10 This model is well accepted, but some other studies showed that the "threepoint" interaction is not a necessity for chiral recognition. 11,12 Booth et al. also tried to explain chiral recognition based on a "conformationally driven" process. 13,14 It was also shown that presence of noncovalent intermolecular interactions (e.g., hydrogen bonding or electrostatic interaction) can induce homochirality to polymeric helical structures when small chiral molecules are present in their self-assembly environment, 15-18 and different chiral selectors were used to selectively separate

the enantiomers of several chiral molecules. <sup>12,19</sup> Despite all these studies and some other theories presented, <sup>20,21</sup> the origin of the homochirality in the early stages of life remains a topic of exploration.

To avoid the complexity of biological systems, in this work, we use structurally well-defined chiral macroions as models to understand the role of chiral counterions on their self-assembly behavior in dilute solution. Macroions are soluble ions with 1-6 nm in size, for example, polyoxometalate clusters, metal organic cages (MOCs) and dendrimers, 22-24 so that their solutions cannot be described by either Debye-Hückel theory<sup>25</sup> for simple ions or Derjaguin, Landau, Vervey, Overbeek (DLVO)<sup>26</sup> theory for colloids. When macroions carry moderate charges, counterion-mediated attraction can overcome their repulsions, leading to a delicate balance and self-assembly behavior. A common assembly structure for relatively isotropic macroions is the thermodynamically stable, single-layered, hollow spherical blackberry-type structure, with the assembly size being determined by the strength of the intermacroionic interactions.<sup>27</sup> In a less polar solvent or higher

Received: August 13, 2020 Revised: October 5, 2020 Published: October 21, 2020





solution ionic strength, the stronger attraction between macroions results in a smaller curvature, that is, a larger assembly size.<sup>23</sup>

MOCs, <sup>28–34</sup> a large group of compounds formed by coordination bonds between transition-metal ions and electron donor organic ligands, are often macroions in solution. The tunable functionality of ligands, size of pores, and structures of MOCs have gained considerable attention in catalysis, <sup>35</sup> imaging and drug delivery, <sup>36,37</sup> sensing, <sup>38,39</sup> and other applications. <sup>40–43</sup> Some MOC macrocations were found to self-assemble into the blackberry structure. <sup>44–47</sup> Similar to other macroions, the assembly size can be reversibly tuned by solvent polarity or adding extra electrolytes. Chirality can be easily induced into the MOCs, <sup>48</sup> making them ideal models for studying the effect of chirality on the intermolecular interactions. It is needed to clarify that, in this paper, the term "synthesis" is used for the coordination reaction between the Pd<sup>2+</sup> ions and the ligands forming MOCs, and "self-assembly" is used for the association of MOCs forming supramolecular structures such as blackberry structures.

We showed that two enantiomeric macroions tend to selfassemble individually instead of forming mixed blackberry structures in their racemic solution. Besides, we very recently indicated that chiral co-ions are able to change the selfassembly behavior of macroions through a solvent shell breakage-related process, while chiral counterions induce these changes by different counterion-macroion association.<sup>4</sup> Given the importance of the counterions in this phenomenon, it would be more interesting to explore how the chiral macroions behave in the presence of chiral counterions. Do the chiral macroions behave similarly when different enantiomeric counterions are present? If not, how different is their behavior and why does this difference exist? Such questions are fundamentally important as they mimic some scenarios of natural processes, such as the protein formation/assembly and the origin of the homochirality.

Herein, we use two enantiomers of  $Pd_{12}L_{24}$  MOC (D- $Pd_{12}L_{24}$  and L- $Pd_{12}L_{24}$ ) with cuboctahedral symmetry and bearing BocD(L)-Ala in their ligands to study the chiral counterion—chiral macroion interaction. The MOCs are originally balanced by simple nitrate counterions to self-assemble into blackberry structures driven by the electrostatic interaction as the major driving force. <sup>50</sup>

#### METHODS

**Materials.** D-Pd<sub>12</sub>L<sub>24</sub> and L-Pd<sub>12</sub>L<sub>24</sub> MOCs with nitrate counterions were synthesized in dimethyl sulfoxide (DMSO), according to the literature. The concentration of each stock solution was 11.27 mg/mL. Solvents, potassium nitrate (KNO<sub>3</sub>), and palladium nitrate (Pd(NO<sub>3</sub>)<sub>2</sub>) were purchased from Sigma-Aldrich. Water was purified by the Milli-Q Direct-Q3 water purification system.

**Sample Preparation.** Concentrated stock solutions were used to prepare dilute solutions. The conditions used for the self-assembly of cages were a 0.5 mg/mL concentration and  $Pd(NO_3)_2/Pd_{12}L_{24}$  ratio of 36, and the desired amount of chiral counterions was added to samples. In order to self-assemble, all of the prepared samples were stored at 50 °C. The solvents and solutions used were dust-freed by Millipore MILLEX-LG 0.20  $\mu$ m PTFE filters.

Static Light Scattering and Dynamic Light Scattering. A commercial Brookhaven Instrument light scattering spectrometer, equipped with a solid-state laser (model

Compass 215M) operating at 532 nm and a BI 9000AT digital correlator, was used for both the static light scattering (SLS) and dynamic light scattering (DLS) measurements. The instrument can detect over an angular range of 15–155°. The temperature of the sample chamber was maintained at 50  $\pm$  0.1 °C during the measurements. The particle average hydrodynamic radius ( $R_{\rm h}$ ) could be obtained by DLS measurements, analyzed by the CONTIN method  $^{52}$  (gamma range: from 100 to 106), and the scattered intensity and radius of gyration ( $R_{\rm g}$ ) can be determined by SLS measurements. In SLS measurements, data were collected either automatically by instrument or manually every 2° between 30 and 120° and analyzed based on Rayleigh–Gans–Debye equation, giving  $R_{\rm g}$  values of the assembly structures in solutions.

**Nuclear Magnetic Resonance Spectroscopy.** All <sup>1</sup>H and <sup>13</sup>C NMR measurements in the liquid state were measured on a Varian NMRS 500 spectrometer, equipped with a 5 mm dual broad-band probe. Baseline correction and noise reduction were performed when appropriate. All spectra were taken at 25.0 °C. For <sup>1</sup>H and <sup>13</sup>C NMR relaxation time was 1 s and 2 s, and number of scans was 64 and 2000, respectively.

For DOSY NMR experiments, the acquisition time was 3 s, the spectral window was 16 ppm (-2 to 14 ppm), the relaxation delay was 6 s, the number of scans was 16, and the number of steady-state (or preacquisition) scans was 16.

ITC Measurements. The isothermal titration calorimetry (ITC) measurements were conducted on a commercial TA Instruments Nano ITC system. The instrument was equipped with a 1.0 mL sample cell and an identical reference cell with an adiabatic shield in a vacuum-tight chamber. For a typical experiment, 1.0 mL of Pd<sub>12</sub>L<sub>24</sub> solution was loaded into the sample cell, and the reference cell was filled with 1.0 mL of DMSO. The salt solution was loaded into a 250  $\mu L$  titration syringe and was titrated into the sample cell with 10  $\mu$ L at each interval. The background heat was subtracted by titrating the same concentration of the salt solution into DMSO. By knowing the concentration of species (Pd<sub>12</sub>L<sub>24</sub>, Pd(NO<sub>3</sub>)<sub>2</sub>, and Boc-Ala in our study) in the cell, their volume for the consecutive titrations, and measuring the released heat of the injection, thermodynamic and binding parameters can be calculated by nonlinear fitting to the independent model. Fitting was performed using NanoAnalyze software provided by TA Instruments. The details about model can be found elsewhere.5

Chirality Confirmation by Circular Dichroism. Far-UV spectra were collected on a circular dichroism (CD) spectrometer (J-1500, Jasco, Easton, MD, USA) in a 1 mm cuvette (J/0556, Jasco). The measurement range was 225–400 nm for the ligand prepared in acetonitrile and 255–400 nm for the cages prepared in DMSO. The measurement was conducted using a data pitch of 0.2, 2 nm bandwidth, a response time of 4 s, and a scan speed of 50 nm/min. The measurement was performed at 25 °C, and six accumulations were averaged for each measurement. Background subtraction and smoothing were performed using Spectra Manager software (Jasco). Data were smoothed using the Means-Movement method with a convolution width of 5.

**Transmission Electron Microscopy.** Regular transmission electron microscopy (TEM) images were taken on a JEOL JEM-1230 electron microscope operated at 120 kV. Samples for regular TEM analysis were prepared by dropping a small volume of solution on a copper grid and fast drying under an oil pump. To improve the visibility of hollow

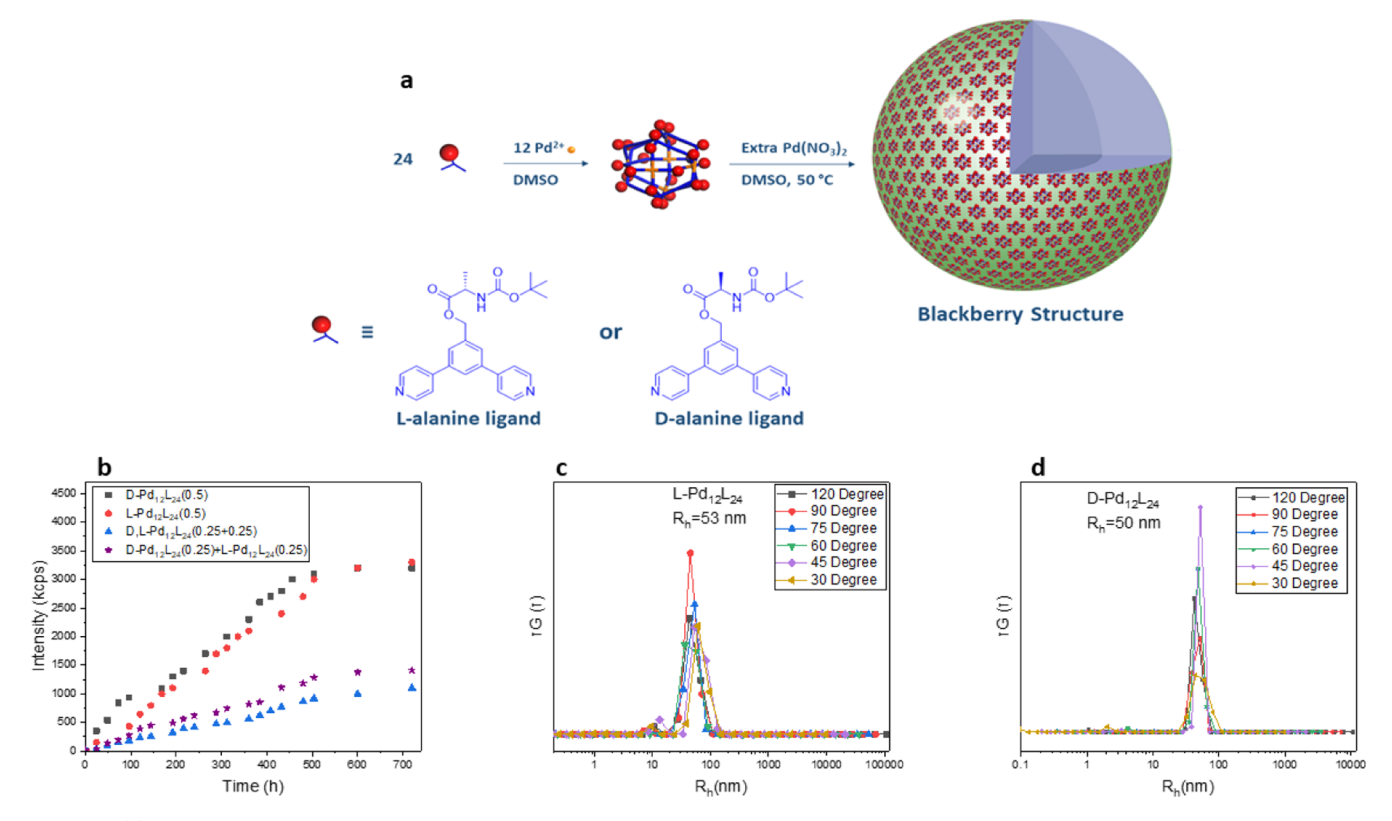


Figure 1. (a) Schematic representation of the synthesis of  $Pd_{12}L_{24}$  MOCs and their self-assembly into hollow spherical blackberry-type structures. (b) Time-resolved scattered intensity measurements for 0.5 mg/mL of pure enantiomeric solutions, their racemic mixture, and intensity summation of 0.25 mg/mL of pure enantiomers. CONTIN analysis results at different scattering angles for the 0.5 mg/mL of (c) L- $Pd_{12}L_{24}$  and (d) D- $Pd_{12}L_{24}$  solutions.

spherical blackberry structures, the contrast and brightness of TEM images were enhanced.

**Matrix-Assisted Laser Desorption/Ionization Time-of-Flight Mass Spectroscopy.** Matrix-assisted laser desorption/ionization time-of-flight (TOF) mass spectra (MS) were measured on a Bruker Ultraflex III TOF/TOF mass spectrometer (Bruker Daltonics). *trans*-2-[3-(4-*tert*-Butylphen-yl)-2-methyl-2-propenylidene]malononitrile was used as the matrix compound. Preparation of the sample was carried out by depositing 0.5  $\mu$ L of matrix solution on the wells of a 384-well ground-steel plate and depositing 0.5  $\mu$ L of sample solution on a spot of the dried matrix, then adding another 0.5  $\mu$ L of matrix solution on top of the dried sample. MS were measured in the reflection mode, and the mass scale was calibrated externally with PS standards with similar molecular weights to those of the samples under consideration. Data analyses were conducted with Bruker's Flex Analysis software.

**Fourier Transform Infrared.** PerkinElmer Spectrum 3 Fourier transform infrared (FT-IR) instrument was used to take the FT-IR spectra of the powdered samples in a 600–4000 cm<sup>-1</sup>wavelength range.

Thermogravimetric Analysis. A TGA 550 by TA instruments was used to generate thermogravimetric analysis (TGA) curves of the powdered samples in a ramp test from room temperature to 500 °C with a heating rate of 15 °C/min.

### ■ RESULTS AND DISCUSSION

Synthesis and Self-Assembly of  $Pd_{12}L_{24}$  MOCs. Two enantiomers of chiral  $Pd_{12}L_{24}$  MOCs, bearing chiral ligands of Boc-L-Ala and Boc-D-Ala, were synthesized separately in DMSO following the reported method in the literature  $^{48,51}$ 

(more details in the Supporting Information).  $Pd_{12}L_{24}$  is a spherical, cage-like coordination complex with 12  $Pd^{2+}$  centers, 24 D- or L-ligand, and 24 nitrate counterions  $^{45,51}$  (Figure 1). Formation of the cages was confirmed using  $^1H$  NMR and  $^1H$  DOSY NMR  $^{54-56}$  (Figures S4 and S5). From the diffusion constants shown in Figure S5 and by using Stokes—Einstein equation,  $^{57}$  the corresponding hydrodynamic radius of D- and L- $Pd_{12}L_{24}$  cages is 2 and 1.9 nm, respectively (details of the calculations can be found in the Supporting Information). The size of the cages is slightly larger than similar cages without alanine in their ligands reported by Fujita previously. The chirality of ligands and cages was confirmed by CD spectra (Figure S7).

 $Pd_{12}L_{24}$  MOCs are not stable in aqueous solutions for a long time;  $^{28,58}$  hence, the self-assembly study was conducted in DMSO. The  $Pd_{12}L_{24}$  solutions with their original nitrate counterions were incubated at 50 °C, and a  $Pd(NO_3)_2/Pd_{12}L_{24}$  ratio of 36 was added to trigger the self-assembly. Figure 1b shows that the scattered intensity from the SLS measurement continuously increases with time, suggesting the continuous supramolecular structure formation. The analysis is based on the simplified Rayleigh–Gans–Debye equation for hollow spheres  $^{59,60}$ 

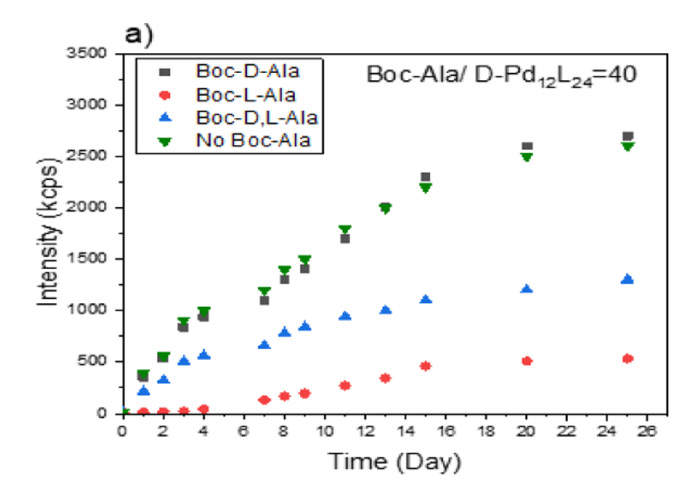
$$I \propto CR_{h,0}^{2} \tag{1}$$

with I, C, and  $R_{\rm h,0}$  being the scattered intensity, the concentration of the assemblies, and hydrodynamic radius of the supramolecular structures at zero scattering angle, respectively. The equation shows that this increment could be due to either the growing concentration of the assemblies or

the increase in their size (or both). The latter possibility is excluded by DLS measurements<sup>61</sup> which shows a mode corresponding to an average hydrodynamic radius  $(R_h)$  of  $\sim 50$  $\pm$  3 nm with narrow size distribution and the  $R_h$  value does not change with time (Figure S10). In addition, the  $R_h$  distribution is angular independent (Figure 1c,d), suggesting that the assemblies are likely isotropic, that is, spherical. Measurement of the radius of gyration  $(R_g)$  from the SLS gave  $R_g/R_h \sim 1$ , revealing that the chiral  $Pd_{12}L_{24}$  cages form hollow spherical blackberry-type structures, <sup>22,23</sup> and TEM images further confirmed the size and spherical shape of the blackberry structures (Figure S11). As shown in Figure 1b, the selfassembly rates for D-Pd<sub>12</sub>L<sub>24</sub> and L-Pd<sub>12</sub>L<sub>24</sub> (black and red curves) in their individual solutions are very similar, and Figure 1c,d indicates that the assembly sizes for the two enantiomers are almost identical, confirming that both enantiomers of Pd<sub>12</sub>L<sub>24</sub> MOCs possess similar self-assembly behaviors, including kinetics in the presence of nitrate counterions.

**Chiral Recognition.** Lower scattered intensity of a racemic mixture of D,L-Pd<sub>12</sub>L<sub>24</sub> 0.25 + 0.25 mg/m (blue symbols shown in Figure 1b, also Figure S12 includes CONTIN analysis), compared to 0.5 mg/mL solutions of pure enantiomeric cages and intensity summation of 0.25 mg/mL of the pure enantiomeric cages, reveals that the collisions between two different enantiomers do not lead to dimer formation thus slowing down the overall self-assembly rate. This is an indirect evidence that chiral recognition occurs during the self-assembly of a racemic mixture solution of the macroions, that is, D-Pd<sub>12</sub>L<sub>24</sub> cages form homochiral blackberry structures together, and L-Pd<sub>12</sub>L<sub>24</sub> cages behave in a similar way. The detailed study of chiral recognition phenomena observed during the self-assembly of chiral macroions can be found in our previous study.

Effect of Boc-Ala Chiral Counterions on the Counterion-Mediated Attraction during the Self-Assembly of Pd<sub>12</sub>L<sub>24</sub> MOCs. The enantiomers of Boc-Ala (the same chiral molecules existing in the ligands of the cages) were introduced into chiral Pd<sub>12</sub>L<sub>24</sub> solutions to investigate their impact on the intermolecular interactions of the cages, and consequently their self-assembly behavior. To 0.5 mg/mL D- or L-Pd<sub>12</sub>L<sub>24</sub> solutions, three different sets of chiral counterions, (1) 40 equiv of Boc-D-Ala, (2) 40 equiv of Boc-L-Ala, and (3) 20 equiv of both Boc-L-Ala and Boc-D-Ala (overall 40 equiv) were added, respectively, and their self-assembly processes were monitored by time-resolved SLS measurements (Figure 2). D-Pd<sub>12</sub>L<sub>24</sub> cages self-assemble quickly in the presence of Boc-D-Ala with a shorter lag phase period (<1 day); however, the selfassembly was slower with a longer lag phase period (~4 days) with Boc-L-Ala as chiral counterions, clearly showing that the enantiomers of the chiral counterion interact differently with the chiral cages. The scattered intensity from D-Pd<sub>12</sub>L<sub>24</sub> solution with the racemic mixture of Boc-Ala stayed between the above two solutions, and the lag phase is <1 day indicating that Boc-D-Ala and Boc-L-Ala still interact differently with the cages. A similar trend was observed for L-Pd<sub>12</sub>L<sub>24</sub>, the presence of Boc-L-Ala led to a fast assembly of the cages; however, Boc-D-Ala drastically decreased the assembly rate with an extended lag phase of almost 4 days. Again, for the racemic mixture of Boc-Ala self-assembly rate stayed between two previous cases (Figure 2b). A longer lag phase period suggests that individual D(L)-Pd<sub>12</sub>L<sub>24</sub> cages are more stable in the solution and have higher tendency to stay as discrete cages when Boc-L(D)-Ala is present.<sup>62</sup> Overall, it can be concluded that Boc-Ala chiral



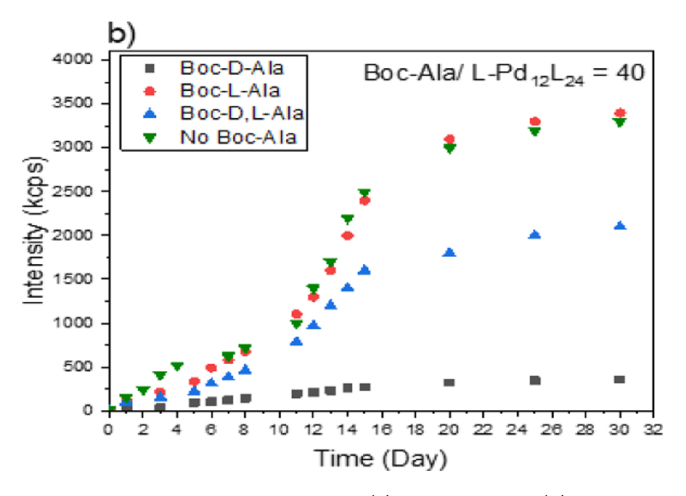
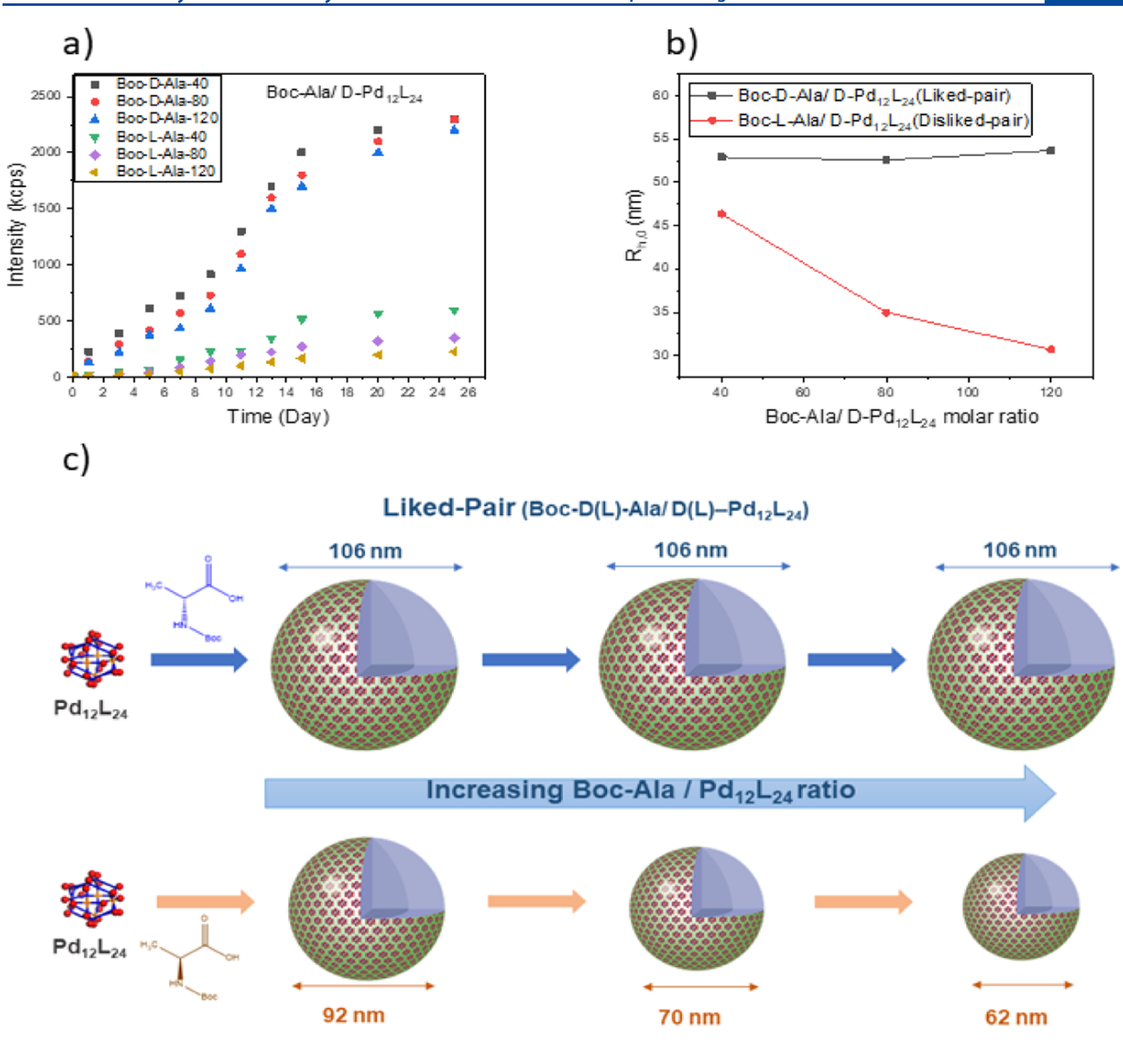


Figure 2. Self-assembly processes of (a)  $D-Pd_{12}L_{24}$  and (b)  $L-Pd_{12}L_{24}$  solutions with or without the addition of chiral Boc-Ala, revealed by time-resolved SLS measurements.

counterions impact the cage—cage intermolecular interactions and their assembly behavior differently. The Boc-L-Ala can weaken the intercage attraction of D-Pd<sub>12</sub>L<sub>24</sub>, resulting in smaller and fewer assemblies, but does not impact the interactions between L-Pd<sub>12</sub>L<sub>24</sub> cages, vice versa for Boc-D-Ala. In the following paragraphs, we will use "liked-pairs" for D-Pd<sub>12</sub>L<sub>24</sub>/Boc-D-Ala and L-Pd<sub>12</sub>L<sub>24</sub>/Boc-L-Ala since the interactions between such pairs do not change the self-assembly behavior of cages, while D-Pd<sub>12</sub>L<sub>24</sub>/Boc-L-Ala and L-Pd<sub>12</sub>L<sub>24</sub>/Boc-D-Ala will be called "disliked-pairs" which would weaken the cage—cage interactions.

In another set of experiments, D-Pd<sub>12</sub>L<sub>24</sub> solutions were prepared with varying molar ratios of Boc-Ala/D-Pd<sub>12</sub>L<sub>24</sub> from 40 to 120 to investigate the reason of lower scattered intensity during the self-assembly of the disliked-pairs. Figure 3a,b shows the scattered intensity increment from time-resolved SLS measurements and their corresponding assembly sizes. It can be seen that the self-assembly speed and the assembly size are very similar for the liked-pairs regardless of the Boc-Ala/Pd<sub>12</sub>L<sub>24</sub> ratio and are also similar to those for the assemblies with only NO<sub>3</sub> counterions (no Boc-Ala). On the other hand, disliked-pairs possess a slower assembly process and smaller assembly size compared with the liked-pairs at the same Boc-Ala/Pd<sub>12</sub>L<sub>24</sub> ratio, as shown in Figure 3c, and this disparity becomes more significant as this ratio increases (e.g., assembly size decreases from 46 to 31 nm).



## Disliked-Pair (Boc-D(L)-Ala/L(D)-Pd<sub>12</sub>L<sub>24</sub>)

Figure 3. (a) Time-resolved SLS measurements during the self-assembly of D-Pd<sub>12</sub>L<sub>24</sub> MOCs in the presence of different amounts of enantiomers of Boc-Ala. A higher Boc-Ala/Pd<sub>12</sub>L<sub>24</sub> molar ratio leads to a slower scattered intensity rise in the disliked-pairs. (b) Size of the blackberry structures vs Boc-Ala/Pd<sub>12</sub>L<sub>24</sub> molar ratio. Higher ratio results in more significant size reduction. (c) Schematic representation of the effect of Boc-Ala on the self-assembly behavior of Pd<sub>12</sub>L<sub>24</sub> when liked-pairs are compared with disliked-pairs.

Based on the assembly size and rate, it can be concluded that the presence of Boc-Ala in a liked-pair does not affect the electrostatic interactions between  $\mathrm{Pd}_{12}\mathrm{L}_{24}$  cages, and the assembly process is energetically as favorable as that with only  $\mathrm{NO_3}^-$  counterions. Meanwhile, in a disliked-pair, the Boc-Ala significantly weakens the attraction between  $\mathrm{Pd}_{12}\mathrm{L}_{24}$  cages, leading to a longer inter- $\mathrm{Pd}_{12}\mathrm{L}_{24}$  distance, consequently a smaller blackberry structure size with a larger curvature. Moreover, a longer lag phase period for the disliked-pairs indicates that the dimer/oligomer formation and whole self-assembly process is energetically less favored.  $^{62,63}$ 

According to eq 1, concentration of the blackberry structures in the case of disliked-pairs is  $33 \pm 2\%$  of the concentration for the liked-pairs at the same Boc-Ala/Pd<sub>12</sub>L<sub>24</sub> molar ratio (40,

80, or 120). The  $\sim$ 67% decrease in the assembly concentration in disliked-pairs is almost constant at different Boc-Ala/Pd<sub>12</sub>L<sub>24</sub> molar ratios, suggesting that the lower scattered intensities for disliked-pairs, when increasing the Boc-Ala/Pd<sub>12</sub>L<sub>24</sub> ratio, is merely due to the smaller size of the assemblies but not fewer assemblies. This means that the presence of more Boc-Ala in a disliked-pair does not lead to more self-assembly suppression but further weakens the attraction between Pd<sub>12</sub>L<sub>24</sub> cages.

Enantiomers of malic acid and tartaric acid showed similar effects on the self-assembly behavior of  $Pd_{12}L_{24}$  cages. Presence of malic acid and tartaric acid in disliked-pairs suppressed the self-assembly process by  $\sim$ 22 and 35%, respectively, when compared to the case of liked-pairs (Figure S20).

To further investigate the interactions between Boc-Ala, Pd(NO<sub>3</sub>)<sub>2</sub>, and chiral Pd<sub>12</sub>L<sub>24</sub> cages, ITC experiments were conducted. The solutions of Pd(NO<sub>3</sub>)<sub>2</sub>, Boc-Ala, and their mixture were slowly titrated into the D- and L-Pd<sub>12</sub>L<sub>24</sub> solutions, where the ion-pair formation between macrocations and small counter-anions (nitrate and Boc-Ala) dominates the process and its thermodynamic parameters can be determined. For this, an independent model was fitted to heat area data after subtracting dilution heat area (generated from titrating Pd(NO<sub>3</sub>)<sub>2</sub>, Boc-Ala, and their mixture into the solvent). Applicability of this model, to calculate thermodynamic and binding parameters of a binding process in which counterions bind to macroions with a single binding site, has been shown in our previous studies. 60,64,65 Here, symmetry of the cage's structure and fitting of the independent model to the data confirms that Pd<sub>12</sub>L<sub>24</sub> cages have only one type of binding site. Within the time scale of ITC experiments, no self-assembly of MOCs occurred. When titrating Boc-Ala [no  $Pd(NO_3)_2$ ] into the Pd<sub>12</sub>L<sub>24</sub> solution, only small heat areas in ITC curve was observed, indicating a weak binding between Boc-Ala and Pd<sub>12</sub>L<sub>24</sub> (Figure S15a). This confirms that Boc-Ala themselves are not capable of triggering the assembly process of Pd<sub>12</sub>L<sub>24</sub> cages, as shown in Figure S14. Negligible heat obtained from titrating Boc-Ala into Pd(NO<sub>3</sub>)<sub>2</sub> ruled out any significant binding between them, for example, complexation (Figure S15b).

Analysis of ITC curves for titrating  $Pd(NO_3)_2$  into the D- or L- $Pd_{12}L_{24}$  cages resulted in a binding number (n) of  $20 \pm 3$ , that is,  $20 \pm 3$  nitrate anions bound to  $Pd_{12}L_{24}$  cages during the process. The high value for binding affinity,  $K_a$ ,  $(\sim 50,000~M^{-1})$  reveals a strong binding between nitrate and  $Pd_{12}L_{24}$ , and the Gibbs free energy is highly negative  $(\sim -29~kJ/mol)$ , indicating that it is a spontaneous binding process (Figure S16 and Table 1). As expected, binding parameters of nitrate to D- $Pd_{12}L_{24}$  and L- $Pd_{12}L_{24}$  are similar since both showed a similar self-assembly behavior (Figure 1).

Table 1. Summary of the Binding and Thermodynamic Parameters during Titration of Small Anions into  $Pd_{12}L_{24}$  Macrocations Obtained by ITC Experiments

	n	$K_a (M^{-1})$	$\Delta G$ (kJ/mol)
$Pd(NO_3)_2/D-Pd_{12}L_{24}$	17.5	$5.13 \times 10^4$	-29.1
$Pd(NO_3)_2 + Boc-D-Ala/D-Pd_{12}L_{24}$	24.9	$5.51 \times 10^4$	-29.3
$Pd(NO_3)_2 + Boc-L-Ala/D-Pd_{12}L_{24}$	11.4	$1.89 \times 10^{4}$	-24.4
$Pd(NO_3)_2/L-Pd_{12}L_{24}$	23.2	$4.27 \times 10^4$	-28.7
$Pd(NO_3)_2 + Boc-L-Ala/L-Pd_{12}L_{24}$	21.2	$5.71 \times 10^4$	-29.4
$Pd(NO_3)_2 + Boc-d-Ala/L-Pd_{12}L_{24}$	12.9	$1.55 \times 10^4$	-25.33

When titrating the mixtures of  $Pd(NO_3)_2$  and Boc-D(L)-Ala into D- $Pd_{12}L_{24}$  solutions, the binding parameters obtained for the liked-pairs (titrating the mixture of  $Pd(NO_3)_2$  and Boc-D-Ala into D- $Pd_{12}L_{24}$ ) are comparable with those for  $Pd(NO_3)_2/Pd_{12}L_{24}$ ; however, for the disliked-pairs, it was observed that the n value decreased from 24.9 to 11.4,  $K_a$  showed a drastic decline from 55,100 to 18,900  $M^{-1}$  and free energy became less negative, changing from -29.3 to -26.4 kJ/mol (Figure 4). Figure S17 and Table 1 show that a similar trend exists for titrating mixtures of  $Pd(NO_3)_2$  and enantiomers of Boc-Ala into L- $Pd_{12}L_{24}$  solutions when the liked-pair was compared to the disliked-pairs. It is obvious that the presence of Boc-Ala in the disliked-pairs strongly affects the binding process between nitrate counterions and  $Pd_{12}L_{24}$ . Fewer counterions (specifi-

cally nitrates) are capable of binding to the  $Pd_{12}L_{24}$  cages with less affinity, and the binding process becomes less spontaneous, that is, thermodynamically less favored.

ITC results confirm that different self-assembly behavior of the liked-pairs and disliked-pairs observed in laser light scattering (LLS) measurements is due to the different counterion— $Pd_{12}L_{24}$  binding processes. Based on these results, there are two types of interactions during the self-assembly process of chiral  $Pd_{12}L_{24}$  cages when chiral counterions, in addition to the nitrates, are present: (1)  $NO_3^--Pd_{12}L_{24}$  interaction to trigger the self-assembly process of the cages and (2) chiral counterion— $Pd_{12}L_{24}$  interaction, leading to the formation of weakly associated diastereoisomeric pairs (the association of chiral macroion—chiral counterion was shown in our previous study as well<sup>49</sup>). Although the latter interaction is weaker than the former one, it determines the difference between the liked-pairs and disliked-pairs during the self-assembly process.

In order to determine whether the interaction between Boc-Ala and Pd<sub>12</sub>L<sub>24</sub> is stronger in a liked-pair or in a disliked-pair, <sup>1</sup>H DOSY NMR of D-Pd<sub>12</sub>L<sub>24</sub> was used as a sufficient tool to compare the strength of intermolecular interactions.  $^{66-68}$  In addition to D-Pd<sub>12</sub>L<sub>24</sub>, a molar ratio of 40 of Boc-D-Ala and Boc-L-Ala and their mixture (20 times of each enantiomer) was added to the solution (Figure S19). Diffusion constant belonging to the closest proton to the chiral center in the ligands (labeled with "f" in Figures S5 and S19) was chosen as a basis for comparison. Lower diffusion constant in the disliked-pair  $(0.4930 \times 10^{-10} \text{ m}^2 \cdot \text{s}^{-1})$  and the solution containing mixture of the enantiomers of Boc-Ala (0.5236 ×  $10^{-10} \text{ m}^2 \cdot \text{s}^{-1}$ ), compared to the liked-pair (0.5766 ×  $10^{-10} \text{ m}^2 \cdot$ s<sup>-1</sup>) indicates that Boc-L-Ala decreases the mobility of D-Pd<sub>12</sub>L<sub>24</sub> due to the stronger interaction between Boc-Ala and  $Pd_{12}L_{24}$  cage in the disliked-pairs. Similar conclusion was obtained by Ma and co-workers<sup>69</sup> for phenylalanine-based metal-organic frameworks. The stronger interaction of D-Pd<sub>12</sub>L<sub>24</sub> toward Boc-L-Ala (compared to Boc-D-Ala) certainly involves the hydrogen binding between the free amino acid (chiral counterion) and the amino acid in the ligands. This chiral recognition can occur through a three-point interaction, 10 a conformationally driven process, 14 or any other mechanism.<sup>12</sup> This reveals that higher binding affinity and binding number in a liked-pair is due to the weak interaction between Boc-Ala and Pd<sub>12</sub>L<sub>24</sub>, which cannot be a barrier against the nitrate-Pd<sub>12</sub>L<sub>24</sub>-binding process. On the other hand, this interaction is stronger in a disliked-pair (although, still weaker than the nitrate-Pd<sub>12</sub>L<sub>24</sub> interaction), which can partially inhibit nitrate-Pd<sub>12</sub>L<sub>24</sub> binding, probably by steric hindrance, and weaken their interaction. The inhibited and weakened nitrate-Pd<sub>12</sub>L<sub>24</sub>-binding process leads to a lower binding affinity and binding number (Table 1), which is the reason of the slower self-assembly process, lower concentration of the assemblies at equilibrium, and their smaller size observed in LLS measurements.

## CONCLUSIONS

The self-assembly process of chiral cationic  $Pd_{12}L_{24}$  MOCs into hollow spherical blackberry-type structures, triggered by the counterion-mediated attraction through the addition of nitrate anions, was used to understand the interaction between chiral macroions and chiral counterions. Enantiomers of Boc-Ala, malic acid, and tartaric acid were introduced into the self-assembly environment as weakly associated chiral counterions.

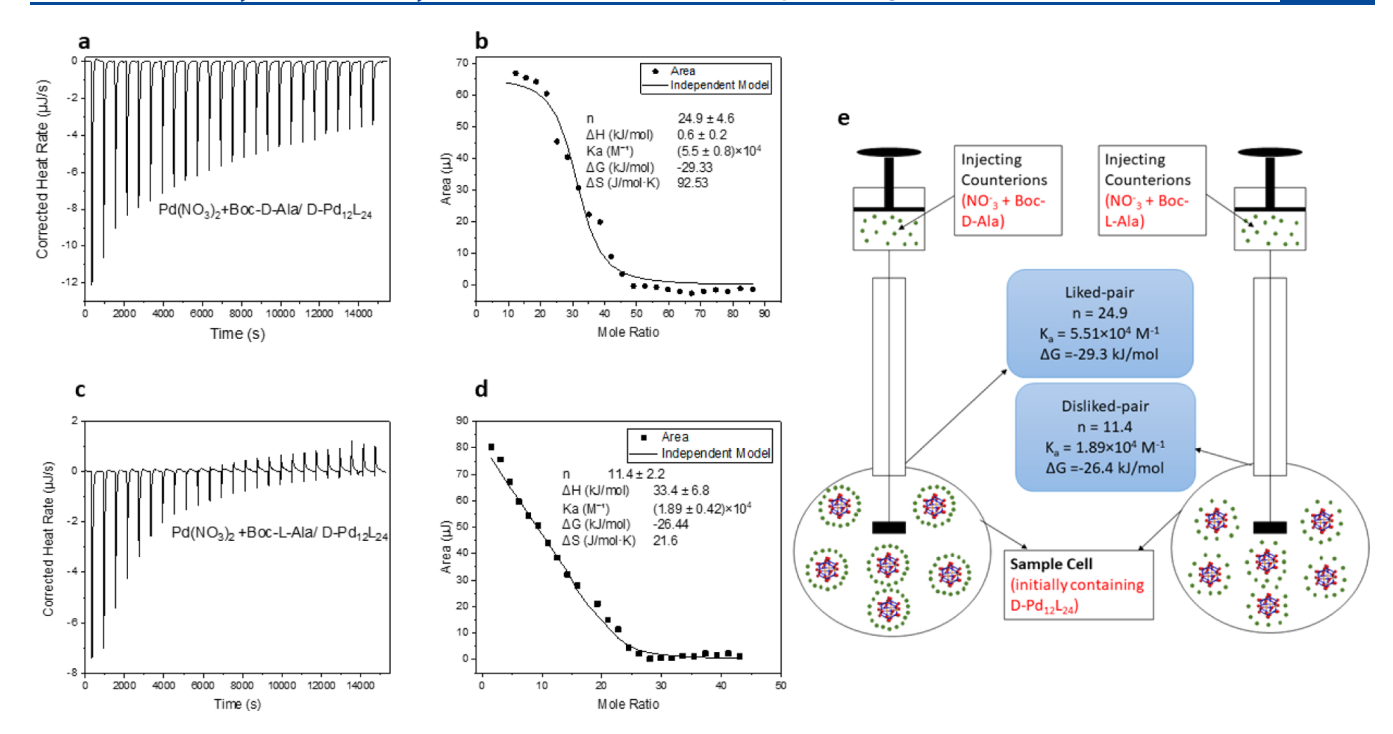


Figure 4. Thermograms and fitting curves by independent model from ITC measurements for titrating (a,b) Boc-D-Ala and  $Pd(NO_3)_2$  (liked-pair) and (c,d) Boc-L-Ala and  $Pd(NO_3)_2$  (disliked-pair) to D- $Pd_{12}L_{24}$ . (e) Schematic demonstration of ITC instrument setup representing different binding parameters of the counterions to chiral  $Pd_{12}L_{24}$  in liked-pairs and disliked-pairs (for clarification  $Pd^{2+}$  ions are omitted and both counterions, nitrate and Boc-Ala, are shown in green).

LLS, ITC, and  $^{1}$ H DOSY NMR results indicated that chiral counterion-chiral  $Pd_{12}L_{24}$  association is stronger in disliked-pairs, compared to liked-pairs, leading to weaker counterion-mediated attraction between the nitrates and  $Pd_{12}L_{24}$ , and inhibits nitrate— $Pd_{12}L_{24}$  binding. As a result of this, different self-assembly behavior, including smaller assembly size, slower self-assembly process, and lower concentration of the assemblies, is observed in disliked-pairs.

## ASSOCIATED CONTENT

## **Supporting Information**

The Supporting Information is available free of charge at https://pubs.acs.org/doi/10.1021/acs.jpcb.0c07424.

Synthesis procedures; <sup>1</sup>H NMR and <sup>13</sup>C NMR spectra of D- and L-ligands; TOF-MS of the enantiomers of the ligands; <sup>1</sup>H NMR and <sup>1</sup>H DOSY NMR spectra of both enantiomers of Pd<sub>12</sub>L<sub>24</sub>; <sup>13</sup>C NMR spectra of D- and L-Pd<sub>12</sub>L<sub>24</sub>; CD spectra of chiral D- and L-ligands and D- and L-Pd<sub>12</sub>L<sub>24</sub> MOCs; FT-IR spectroscopy of D- and L-Pd<sub>12</sub>L<sub>24</sub> MOCs; TGA curves of L- and D-Pd<sub>12</sub>L<sub>24</sub>; CONTIN analysis of the self-assembled blackberry structures; SLS data for Pd<sub>12</sub>L<sub>24</sub> with different concentrations; time-resolved SLS measurements of D-Pd<sub>12</sub>L<sub>24</sub> MOCs; ITC measurements and fitted data to independent model for heat area data; stability test of Pd<sub>12</sub>L<sub>24</sub> cages in the presence of Boc-Ala by <sup>1</sup>H NMR; and <sup>1</sup>H NMR DOSY data (PDF)

## AUTHOR INFORMATION

## **Corresponding Author**

Tianbo Liu — Department of Polymer Science, The University of Akron, Akron, Ohio 44325, United States; oorcid.org/0000-

0002-8181-1790; Phone: (+1)330-972-3496; Email: tliu@uakron.edu

#### **Authors**

Ehsan Raee — Department of Polymer Science, The University of Akron, Akron, Ohio 44325, United States; ⑤ orcid.org/0000-0001-8123-2062

Hui Li – Department of Polymer Science, The University of Akron, Akron, Ohio 44325, United States

Xinyu Sun — Department of Polymer Science, The University of Akron, Akron, Ohio 44325, United States; orcid.org/0000-0003-4353-1832

Putu Ustriyana — Department of Polymer Science, The University of Akron, Akron, Ohio 44325, United States; orcid.org/0000-0001-9804-3081

**Jiancheng Luo** – Department of Polymer Science, The University of Akron, Akron, Ohio 44325, United States

Jiahui Chen − Department of Polymer Science, The University of Akron, Akron, Ohio 44325, United States; orcid.org/0000-0002-3861-146X

Nita Sahai — Department of Polymer Science, The University of Akron, Akron, Ohio 44325, United States; orcid.org/0000-0003-3852-0557

Complete contact information is available at: https://pubs.acs.org/10.1021/acs.jpcb.0c07424

#### Notes

The authors declare no competing financial interest.

#### ACKNOWLEDGMENTS

T.L. acknowledges support by NSF (CHE 1904397), and the University of Akron. N.S. is grateful for generous gift funds from Dr. Edward Weil.

#### REFERENCES

- (1) Pasteur, L. Memoir on the Relationship That Can Exist between Crystalline Form and Chemical Composition, and on the Cause of Rotary Polarization. C. R. Acad. Sci. 1848, 26, 535–538.
- (2) Blackmond, D. G. Autocatalytic Models for the Origin of Biological Homochirality. *Chem. Rev.* **2020**, *120*, 4831–4847.
- (3) Ribó, J. M.; Hochberg, D.; Crusats, J.; El-Hachemi, Z.; Moyano, A. Spontaneous Mirror Symmetry Breaking and Origin of Biological Homochirality. *J. R. Soc. Interface* **2017**, *14*, 20170699.
- (4) Liu, S. Homochirality Originates from the Handedness of Helices. J. Phys. Chem. Lett. 2020, 11, 8690–8696.
- (5) Karunakaran, S. C.; Cafferty, B. J.; Weigert-Muñoz, A.; Schuster, G. B.; Hud, N. V. Spontaneous Symmetry Breaking in the Formation of Supramolecular Polymers: Implications for the Origin of Biological Homochirality. *Angew. Chem. Int. Ed.* **2019**, *58*, 1453–1457.
- (6) Blackmond, D. G. The Origin of Biological Homochirality. *Cold Spring Harbor Perspect. Biol.* **2019**, *11*, a032540.
- (7) Alkorta, I.; Picazo, O.; Elguero, J. Theoretical Studies on Chiral Discrimination. *Curr. Org. Chem.* **2006**, *10*, 695–714.
- (8) Leszczynski, J.; Shukla, M. K. Practical Aspects of Computational Chemistry IV; Springer, 2016.
- (9) Yin, P.; Zhang, Z.-M.; Lv, H.; Li, T.; Haso, F.; Hu, L.; Zhang, B.; Bacsa, J.; Wei, Y.; Gao, Y.; et al. Chiral Recognition and Selection during the Self-Assembly Process of Protein-Mimic Macroanions. *Nat. Commun.* **2015**, *6*, 6475.
- (10) Easson, L. H.; Stedman, E. Studies on the Relationship between Chemical Constitution and Physiological Action: Molecular Dissymmetry and Physiological Activity. *Biochem. J.* 1933, 27, 1257—1266
- (11) Greber, T.; Šljivančanin, Ž.; Schillinger, R.; Wider, J.; Hammer, B. Chiral Recognition of Organic Molecules by Atomic Kinks on Surfaces. *Phys. Rev. Lett.* **2006**, *96*, 056103.
- (12) Berthod, A. Chiral Recognition Mechanisms. *Anal. Chem.* **2006**, 78, 2093–2099.
- (13) Booth, T. D.; Wainer, I. W. Investigation of the Enantioselective Separations of  $\alpha$ -Alkylarylcarboxylic Acids on an Amylose Tris(3,5-Dimethylphenylcarbamate) Chiral Stationary Phase Using Quantitative Structure-Enantioselective Retention Relationships Identification of a Conformation. *J. Chromatogr. A* **1996**, 737, 157–169.
- (14) Booth, T. D.; Wahnon, D.; Wainer, I. W. Is Chiral Recognition a Three-Point Process? *Chirality* **1997**, *9*, 96–98.
- (15) Yashima, E.; Maeda, K.; Okamoto, Y. Memory of Macromolecular Helicity Assisted by Interaction with Achiral Small Molecules. *Nature* **1999**, 399, 449–451.
- (16) Kumar, M.; Brocorens, P.; Tonnelé, C.; Beljonne, D.; Surin, M.; George, S. J. A Dynamic Supramolecular Polymer with Stimuli-Responsive Handedness for in Situ Probing of Enzymatic ATP Hydrolysis. *Nat. Commun.* **2014**, *5*, 5793.
- (17) Fenniri, H.; Deng, B.-L.; Ribbe, A. E. Helical Rosette Nanotubes with Tunable Chiroptical Properties. *J. Am. Chem. Soc.* **2002**, *124*, 11064–11072.
- (18) George, S. J.; Tomović, Ž.; Smulders, M. M. J.; de Greef, T. F. A.; Leclère, P. E. L. G.; Meijer, E. W.; Schenning, A. P. H. J. Helicity Induction and Amplification in an Oligo(p-Phenylenevinylene) Assembly through Hydrogen-Bonded Chiral Acids. *Angew. Chem. Int. Ed.* 2007, 46, 8206–8211.
- (19) Gübitz, G. Separation of Drug Enantiomers by HPLC Using Chiral Stationary Phases A Selective Review. *Chromatographia* **1990**, *30*, 555–564.
- (20) Lough, J.; Wainer, I. W. Chirality in the Natural & Applied Sciences; Blackwell Publishing Limited: Oxford, 2002.
- (21) Gujarro, A.; Yus, M. The Origin of Chirality in the Molecules of Life: A Revision from Awareness to the Current Theories and Perspectives of This Unsolved Problem; RCS Publishing: Cambridge 2009.
- (22) Liu, T.; Diemann, E.; Li, H.; Dress, A. W. M.; Müller, A. Self-Assembly in Aqueous Solution of Wheel-Shaped Mo154 Oxide Clusters into Vesicles. *Nature* **2003**, *426*, 59–62.

- (23) Yin, P.; Li, D.; Liu, T. Solution Behaviors and Self-Assembly of Polyoxometalates as Models of Macroions and Amphiphilic Polyoxometalate—Organic Hybrids as Novel Surfactants. *Chem. Soc. Rev.* **2012**, *41*, 7368–7383.
- (24) Liu, T. Hydrophilic Macroionic Solutions: What Happens When Soluble Ions Reach the Size of Nanometer Scale? *Langmuir* **2010**, *26*, 9202–9213.
- (25) Debye, P.; Hückel, E. De La Theorie Des Electrolytes. I. Abaissement Du Point de Congelation et Phenomenes Associes. *Phys. Z.* **1923**, 24, 185–206.
- (26) Venvey, E. J. W.; Overbeek, J. T. G. Theory of the Stability of Lyophobic Colloids; Elsevier Publishing Company, 1948.
- (27) Luo, J.; Liu, T. Competition and Cooperation among Different Attractive Forces in Solutions of Inorganic—Organic Hybrids Containing Macroionic Clusters. *Langmuir* **2019**, *35*, 7603–7616.
- (28) Tominaga, M.; Suzuki, K.; Kawano, M.; Kusukawa, T.; Ozeki, T.; Sakamoto, S.; Yamaguchi, K.; Fujita, M. Finite, Spherical Coordination Networks That Self-Organize from 36 Small Components. *Angew. Chem. Int. Ed.* **2004**, 43, 5621–5625.
- (29) Harris, K.; Fujita, D.; Fujita, M. Giant Hollow MnL2n Spherical Complexes: Structure, Functionalisation and Applications. *Chem. Commun.* **2013**, 49, 6703–6712.
- (30) Kamiya, N.; Tominaga, M.; Sato, S.; Fujita, M. Saccharide-Coated M12L24 Molecular Spheres That Form Aggregates by Multi-Interaction with Proteins. *J. Am. Chem. Soc.* **2007**, *129*, 3816–3817.
- (31) Kikuchi, T.; Sato, S.; Fujita, M. Well-Defined DNA Nanoparticles Templated by Self-Assembled M12L24 Molecular Spheres and Binding of Complementary Oligonucleotides. *J. Am. Chem. Soc.* **2010**, *1*32, 15930–15932.
- (32) Ikemi, M.; Kikuchi, T.; Matsumura, S.; Shiba, K.; Sato, S.; Fujita, M. Peptide-Coated, Self-Assembled M12L24 Coordination Spheres and Their Immobilization onto an Inorganic Surface. *Chem. Sci.* **2010**, *1*, 68–71.
- (33) Cook, T. R.; Zheng, Y.-R.; Stang, P. J. Metal-Organic Frameworks and Self-Assembled Supramolecular Coordination Complexes: Comparing and Contrasting the Design, Synthesis, and Functionality of Metal-Organic Materials. *Chem. Rev.* **2013**, *113*, 734-777.
- (34) Chakrabarty, R.; Mukherjee, P. S.; Stang, P. J. Supramolecular Coordination: Self-Assembly of Finite Two- and Three-Dimensional Ensembles. *Chem. Rev.* **2011**, *111*, 6810–6918.
- (35) Wang, Q.-Q.; Gonell, S.; Leenders, S. H. A. M.; Dürr, M.; Ivanović-Burmazović, I.; Reek, J. N. H. Self-Assembled Nanospheres with Multiple Endohedral Binding Sites Pre-Organize Catalysts and Substrates for Highly Efficient Reactions. *Nat. Chem.* **2016**, *8*, 225.
- (36) Taylor-Pashow, K. M. L.; Della Rocca, J.; Xie, Z.; Tran, S.; Lin, W. Postsynthetic Modifications of Iron-Carboxylate Nanoscale Metal—Organic Frameworks for Imaging and Drug Delivery. *J. Am. Chem. Soc.* **2009**, *131*, 14261–14263.
- (37) Zhao, D.; Tan, S.; Yuan, D.; Lu, W.; Rezenom, Y. H.; Jiang, H.; Wang, L.-Q.; Zhou, H.-C. Surface Functionalization of Porous Coordination Nanocages Via Click Chemistry and Their Application in Drug Delivery. *Adv. Mater.* **2011**, *23*, 90–93.
- (38) Qiu, S.; Zhu, G. Molecular Engineering for Synthesizing Novel Structures of Metal—Organic Frameworks with Multifunctional Properties. *Coord. Chem. Rev.* **2009**, 253, 2891–2911.
- (39) Zhang, M.; Saha, M. L.; Wang, M.; Zhou, Z.; Song, B.; Lu, C.; Yan, X.; Li, X.; Huang, F.; Yin, S.; et al. Multicomponent Platinum(II) Cages with Tunable Emission and Amino Acid Sensing. *J. Am. Chem. Soc.* 2017, 139, 5067–5074.
- (40) Inokuma, Y.; Kawano, M.; Fujita, M. Crystalline Molecular Flasks. *Nat. Chem.* **2011**, *3*, 349.
- (41) Chen, L.-J.; Ren, Y.-Y.; Wu, N.-W.; Sun, B.; Ma, J.-Q.; Zhang, L.; Tan, H.; Liu, M.; Li, X.; Yang, H.-B. Hierarchical Self-Assembly of Discrete Organoplatinum(II) Metallacycles with Polysaccharide via Electrostatic Interactions and Their Application for Heparin Detection. *J. Am. Chem. Soc.* **2015**, *137*, 11725–11735.

- (42) Garberoglio, G.; Skoulidas, A. I.; Johnson, J. K. Adsorption of Gases in Metal Organic Materials: Comparison of Simulations and Experiments. *J. Phys. Chem. B* **2005**, *109*, 13094–13103.
- (43) Keskin, S.; Liu, J.; Rankin, R. B.; Johnson, J. K.; Sholl, D. S. Progress, Opportunities, and Challenges for Applying Atomically Detailed Modeling to Molecular Adsorption and Transport in Metal—Organic Framework Materials. *Ind. Eng. Chem. Res.* **2009**, *48*, 2355—2371.
- (44) Li, D.; Zhang, J.; Landskron, K.; Liu, T. Spontaneous Self-Assembly of Metal—Organic Cationic Nanocages to Form Monodisperse Hollow Vesicles in Dilute Solutions. *J. Am. Chem. Soc.* **2008**, 130, 4226—4227.
- (45) Li, H.; Luo, J.; Liu, T. Modification of the Solution Behavior of Pd12L24 Metal—Organic Nanocages via PEGylation. *Chem.—Eur. J.* **2016**, 22, 17949—17952.
- (46) Li, H.; Xie, T.-Z.; Liang, Z.; Shen, Y.; Sun, X.; Yang, Y.; Liu, T. Adjusting Emission Wavelength by Tuning the Intermolecular Distance in Charge-Regulated Supramolecular Assemblies. *J. Phys. Chem. C* 2019, 123, 23280–23286.
- (47) Li, H.; Wang, R.; Hong, Y. I.; Liang, Z.; Shen, Y.; Nishiyama, Y.; Miyoshi, T.; Liu, T. Tuning the Intercage Distance in Charge-Regulated Blackberry-Type Assemblies through Host—Guest Chemistry. *Chem.—Eur. J.* **2019**, *25*, 5803–5808.
- (48) Suzuki, K.; Kawano, M.; Sato, S.; Fujita, M. Endohedral Peptide Lining of a Self-Assembled Molecular Sphere To Generate Chirality-Confined Hollows. J. Am. Chem. Soc. 2007, 129, 10652–10653.
- (49) Luo, J.; Ye, S.; Ustriyana, P.; Wei, B.; Chen, J.; Raee, E.; Hu, Y.; Yang, Y.; Zhou, Y.; Wesdemiotis, C.; et al. Unraveling Chiral Selection in the Self-Assembly of Chiral Fullerene Macroions: Effects of Small Chiral Components Including Counterions, Co-Ions, or Neutral Molecules. *Langmuir* **2020**, *36*, 4702–4710.
- (50) Li, D.; Zhou, W.; Landskron, K.; Sato, S.; Kiely, C. J.; Fujita, M.; Liu, T. Viral-Capsid-Type Vesicle-Like Structures Assembled from M12L24 Metal—Organic Hybrid Nanocages. *Angew. Chem. Int. Ed.* **2011**, *50*, 5182–5187.
- (51) Zhukhovitskiy, A. V.; Zhong, M.; Keeler, E. G.; Michaelis, V. K.; Sun, J. E. P.; Hore, M. J. A.; Pochan, D. J.; Griffin, R. G.; Willard, A. P.; Johnson, J. A. Highly Branched and Loop-Rich Gels via Formation of Metal—Organic Cages Linked by Polymers. *Nat. Chem.* **2015**, *8*, 33.
- (52) Provencher, S. W. Fourier Method for the Analysis of Exponential Decay Curves. *Biophys. J.* **1976**, *16*, 27–41.
- (53) Velazquez-Campoy, A.; Leavitt, S. A.; Freire, E. Characterization of Protein-Protein Interactions by Isothermal Titration Calorimetry BT—Protein-Protein Interactions: Methods and Applications; Meyerkord, C. L., Fu, H., Eds.; Springer New York: New York, NY, 2015; pp 183–204.
- (54) Li, K.; Zhang, L.-Y.; Yan, C.; Wei, S.-C.; Pan, M.; Zhang, L.; Su, C.-Y. Stepwise Assembly of Pd6(RuL3)8 Nanoscale Rhombododecahedral Metal—Organic Cages via Metalloligand Strategy for Guest Trapping and Protection. J. Am. Chem. Soc. 2014, 136, 4456–4459.
- (55) Ronson, T. K.; Fisher, J.; Harding, L. P.; Hardie, M. J. Star-Burst Prisms with Cyclotriveratrylene-Type Ligands: A [Pd6L8]12+Stella Octangular Structure. *Angew. Chem. Int. Ed.* **2007**, *46*, 9086–9088.
- (56) Riddell, I. A.; Hristova, Y. R.; Clegg, J. K.; Wood, C. S.; Breiner, B.; Nitschke, J. R. Five Discrete Multinuclear Metal-Organic Assemblies from One Ligand: Deciphering the Effects of Different Templates. J. Am. Chem. Soc. 2013, 135, 2723–2733.
- (57) Dill, K.; Bromberg, S. Molecular Driving Forces: Statistical Thermodynamics in Biology, Chemistry, Physics, and Nanoscience; Garland Science, 2012.
- (58) Tominaga, M.; Suzuki, K.; Murase, T.; Fujita, M. 24-Fold Endohedral Functionalization of a Self-Assembled M12L24 Coordination Nanoball. *J. Am. Chem. Soc.* **2005**, *127*, 11950–11951.
- (59) Hiemenz, P. C.; Rajagopalan, R. Principles of Colloid and Surface Chemistry; The Electrical Double Layer and Double-Layer Interactions; Marcel Dekker Inc., 1997; pp 499–533.

- (60) Luo, J.; Chen, K.; Yin, P.; Li, T.; Wan, G.; Zhang, J.; Ye, S.; Bi, X.; Pang, Y.; Wei, Y.; Liu, T. Effect of Cation– $\pi$  Interaction on Macroionic Self-Assembly. *Angew. Chem.* **2018**, *130*, 4131–4136.
- (61) Provencher, S. W. CONTIN: A General Purpose Constrained Regularization Program for Inverting Noisy Linear Algebraic and Integral Equations. *Comput. Phys. Commun.* **1982**, *27*, 229–242.
- (62) Zhang, J.; Li, D.; Liu, G.; Glover, K. J.; Liu, T. Lag Periods During the Self-Assembly of {Mo72Fe30} Macroions: Connection to the Virus Capsid Formation Process. J. Am. Chem. Soc. 2009, 131, 15152–15159.
- (63) Liu, G.; Liu, T.; Mal, S. S.; Kortz, U. Wheel-Shaped Polyoxotungstate [Cu20Cl(OH)24(H2O)12(P8W48O184)]25-Macroanions Form Supramolecular "Blackberry" Structure in Aqueous Solution. *I. Am. Chem. Soc.* **2006**, *128*, 10103–10110.
- (64) He, J.; Li, H.; Yang, P.; Haso, F.; Wu, J.; Li, T.; Kortz, U.; Liu, T. Tuning of Polyoxopalladate Macroanionic Hydration Shell via Countercation Interaction. *Chem.—Eur. J.* **2018**, *24*, 3052–3057.
- (65) Luo, J.; Ye, S.; Li, T.; Sarnello, E.; Li, H.; Liu, T. Distinctive Trend of Metal Binding Affinity via Hydration Shell Breakage in Nanoconfined Cavity. *J. Phys. Chem. C* **2019**, *123*, 14825–14833.
- (66) Brand, T.; Cabrita, E. J.; Berger, S. Intermolecular Interaction as Investigated by NOE and Diffusion Studies. *Prog. Nucl. Magn. Reson. Spectrosc.* **2005**, *46*, 159–196.
- (67) Pagès, G.; Gilard, V.; Martino, R.; Malet-Martino, M. Pulsed-Field Gradient Nuclear Magnetic Resonance Measurements (PFG NMR) for Diffusion Ordered Spectroscopy (DOSY) Mapping. *Analyst* **2017**, *142*, 3771–3796.
- (68) Avram, L.; Cohen, Y. Diffusion NMR of Molecular Cages and Capsules. *Chem. Soc. Rev.* **2015**, *44*, 586–602.
- (69) Ma, X.; Zhang, Y.; Gao, Y.; Li, X.; Wang, C.; Yuan, H.; Yu, A.; Zhang, S.; Cui, Y. Revelation of the Chiral Recognition of Alanine and Leucine in an L-Phenylalanine-Based Metal—Organic Framework. *Chem. Commun.* **2020**, *56*, 1034—1037.